Materials Research Proceedings 44 (2024) 548-557 https://doi.org/10.21741/9781644903254-59

Development of unified constitutive model for hot deformation behavior of TC4 with and without diffusion bonding

CAI Zhongman[1,a], CHEN Haosheng[1,b], LI Can[1,c], CHEN Jiarui[1,d], LI Xiaoxing[1,e] and LI Yong[1,f*]

[1]Beihang University XueYuan Road No.37, Haidian District, Beijing, China

[a]czmncst@163.com, [b]chenhs@buaa.edu.cn, [c]lican9504@163.com, [d]jiaruic@buaa.edu.cn, [e]li.xiaoxing@buaa.edu.cn, [f]liyong19@buaa.edu.cn

Keywords: TC4, Hot Deformation, Modeling, Diffusion Bonding

Abstract. The hot deformation behavior of TC4 with and without diffusion bonding (DB) is studied. Firstly, the hot tensile testes of TC4 specimens with and without DB were carried out at temperature of 750℃ and strain rate of 0.1 ~ 0.0001 s^{-1}. It was found that the peak stress and fracture strain of DB specimens are lower than those of base metal (BM) specimens. The quasi-cleavage fracture appeared in the DB specimens at 750℃, and the mechanism could be explained as straight grain boundary formed by incomplete recrystallization and insufficient grain boundary migration energy and the joints weak left over from the DB process causing rapid voids nucleation at the DB interface. The shorter distance of voids coalescence within the interface leads to quasi-cleavage fracture. In addition, a unified constitutive model based on internal variables was developed by introducing the weld-dependent fracture coefficients and damage tolerance coefficient. The model can accurately predict the hot deformation behavior of TC4 with and without diffusion bonding, describing the influence behavior of DB area on hot deformation, as well as the evolutions of internal variables, including dislocation density, reserve fraction, dynamic recrystallization (DRX) fraction and damage. It provides a theoretical basis for further accurate simulation of the hot forming of titanium alloy with diffusion bonding.

Introduction

TC4 titanium alloy has been widely used in aerospace engineering, vehicle engineering and medical fields [1, 2]. TC4 hollow parts have low material density and higher hollowness, which highlights its lightweight characteristics. The main manufacturing processes of hollow parts are integral casting, additive manufacturing, and diffusion bonding (DB). Compared with integral casting and additive manufacturing, DB has the advantages of easy control of process parameters, small deformation, higher dimensional accuracy and mechanical properties of welded joints that are equivalent to those of base metal (BM). At present, superplastic forming and diffusion bonding (SPF/DB) or hot forming and DB hybrid processes are often used for hollow blade manufacturing [3]. On the basis of DB, subsequent forming is carried out to obtain the final part. In the process of hot forming, the deformation is large and the relationship of microstructure evolution is more complicated. The alloy is very sensitive to the initial state [4]. Different initial states also lead to different deformation behaviors in subsequence processing. Therefore, it is important and necessary to characterize and realize the hot deformation characteristics of materials after DB.

Guo and Peng [5] studied the welding and microstructure evolution during TC4 diffusion bonding. Two states will be formed at the interface: one is that the recrystallized grains pass through the original interface and replace, and the other is that the recrystallized grains form a new straight grain boundary at the interface. Li and Imran [5] conducted tensile tests on TC4 with DB specimens and found that the elongation of TC4 with DB was lower than BM at elevated temperatures. Li [3] studied the microstructure evolution of tc4 at hot temperatures and believed that the temperature required for DRX to occur at the DB interface was higher. The

characterization of this difference in hot deformation characteristics is of great significance for process optimization and precision manufacturing.

E. Alabort [8] established a unified viscoplastic constitutive model to simulate the superplastic diffusion bonding process of Ti-6Al-4V. It is proved that deformation behavior prediction with processing history information and internal microstructure state is more accurate. Lin[18] applied the internal variable constitutive model of dislocations, grain size and recrystallization variables to TC4 alloy, and achieved good prediction results. On this basis, Bai [19] established a unified constitutive of dislocation and spheroidization behavior and applied it to TC4 alloy. However, the above studies are all based on homogeneous TC4, which does not have the ability to describe the changes of hot deformation characteristics caused by specific structures at the same time.

Therefore, in this work, TC4 in DB and BM states are selected as the original state to study. Firstly, the hot tensile test is carried out at 750℃ and 0.0001 ~ 0.1 s^{-1}, and the hot deformation behavior is analyzed. On this basis, a set of internal variable constitutive model is developed to describe the hot deformation characteristics of both states at the same time. The parameters of the equation will be calibrated by the Particle Swarm Optimization (PSO) algorithm. Finally, the prediction effect is evaluated by statistics.

Material and experimental

The as-received material is prepared by diffusion welding of two TC4 alloy plates, as shown in Fig. 1(a). On the welding material, DB and BM round bar tensile specimens with a diameter of 3 mm and a gauge distance of 15mm are made along the thickness direction and length direction, respectively, as shown in Fig. 1(b). The temperature is selected as 750℃, TC4 conventional thermoforming processing temperature. The strain rates are 0.1,0.01,0.001, 0.0001s^{-1}.

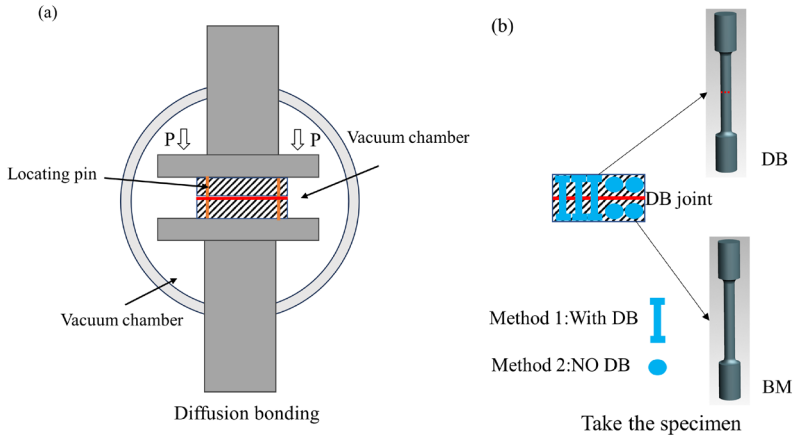

Fig. 1. (a) Billet diffusion welding diagram and (b) specimen preparation diagram.

Experimental results and discussions

The flow stress-strain curves comparison of TC4 between BM and DB states is shown in Fig. 2 (a). Comparing the two can be found that the stress-strain curves of BM have a higher peak stress at the beginning of deformation, as shown in the pink dotted circle. The peak stresses are plotted as shown in Fig. 2(b) It can be found that with the increase of strain rate, the difference of peak stress between BM and DB becomes smaller. The DB process of TC4 is studied in reference [5]. The results show that the DRX will occur at the interface during DB, which will lead to a decrease of dislocation density. The dislocation density of the BM specimen is higher, which makes the dislocation accumulation and entanglement more intense. Work hardening is strengthened, making the stress required for deformation greater. So the peak stress of BM is greater. With the increase of strain rate, the deformation time is shorter and the dislocation increment rate is larger. Therefore, the effect of the original dislocation density is weakened. This results in the phenomenon that the peak stress difference decreases with the increase of strain rate.

As the deformation continues, the stress of BM softens faster, and the stress gradually approaches. The higher dislocation density allows the DRX behavior to occur earlier and more fully resulting in the softening effect stronger. When the stress is close, such as the position indicated by the red arrow, the DB specimen breaks and the stress is 0. However, the BM specimen continued to deform and gradually decreased to 0. Fig. 2(c) shows the comparison of fracture strain between DB and BM specimens. Due to the rapid fracture of the DB specimen, the fracture strain is lower than that of the BM specimen. The results show that the DB specimen has worse formability than the BM specimen, and it is necessary to pay more attention to its damage behavior.

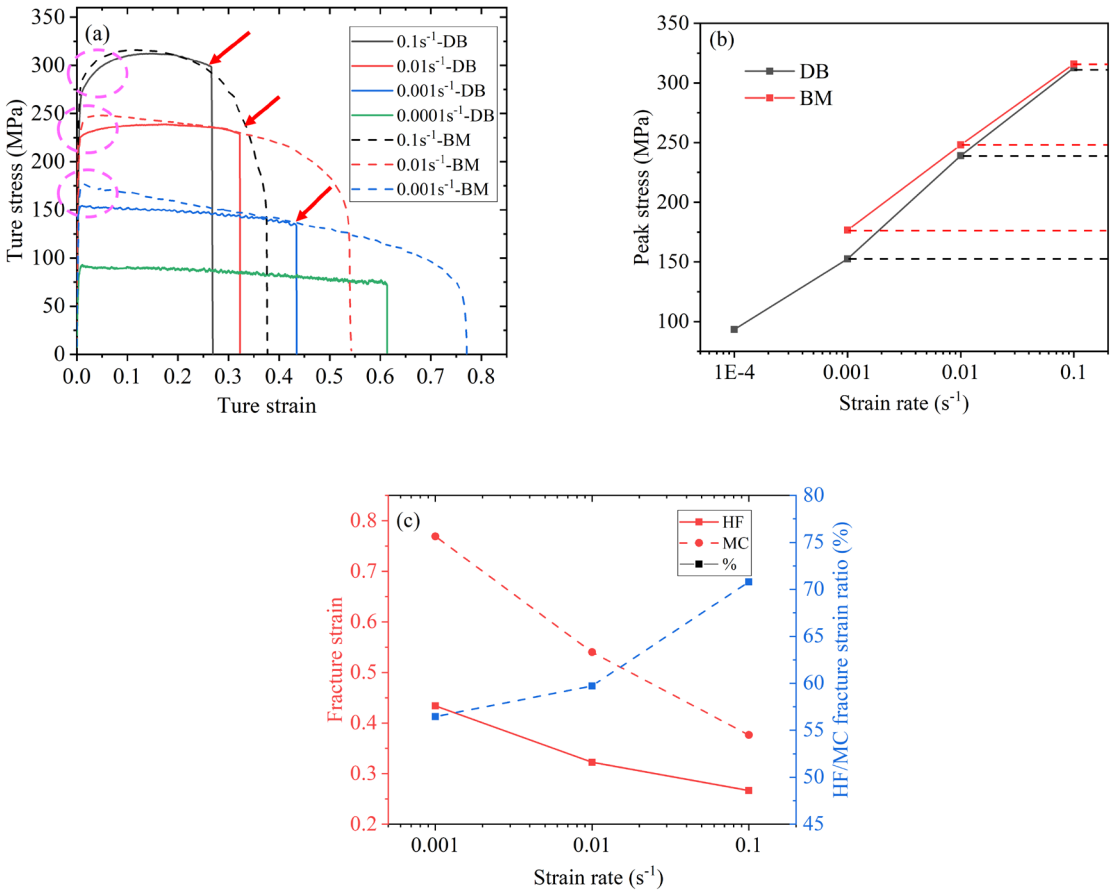

Fig. 2. (a) The flow stress-strain curves of TC4 comparison between BM and DB; (b) peak stress and (c) comparison of fracture strain between DB and BM.

Fig. 3(a) shows the fracture morphology of BM at a strain rate of $0.1s^{-1}$. We can clearly see a necking phenomenon at the fracture. By observing the microstructure of the fracture, a large number of dimples were found. It shows that the fracture of BM is a typical ductile fracture. Fig. 3(b) and (c) show the fractures morphology of DB with strain rates of $0.1s^{-1}$ and $0.0001s^{-1}$, respectively. The whole fracture is straight, and there is no obvious necking phenomenon. By observing the microstructure of the fracture, it is found that dimple and transgranular fracture are the typical characteristics of quasi-cleavage fracture. This indicates that at 750°C, 0.1 ~ 0.0001 s^{-1}, the DB specimen will have quasi-cleavage fracture during hot deformation. Fig. 3 (d) shows the forming mechanism of the fracture at the DB interface on a microscopic scale. Some scholars [5] have shown that during the DB process, the inadequate deformation resulted in incomplete recrystallization and grain boundary migration, the storage energy difference on both sides of the interface was not enough to drive the grain boundary migration process. Therefore, the straight grain boundary formed. The voids preferentially nucleate at the grain boundary [9], and damage is

more likely to occur at the interface. In the process of deformation, the voids are preferently nucleated at the joints weak, impurities, and grain boundaries at the DB interface Resulting in the rapid formation of a large number of voids in the DB interface. Moreover, the voids coalescence distance at the interface is shorter, and it is easier to coalesce with continuous deformation. This results in a quasi-cleavage fracture. This also indicates that the damage of DB specimens is more inclined to coalescence at the interface of DB, resulting in a decrease in fracture strain. In order to simulate this kind of specimen, the damage tolerance is proposed. The hot deformation and fracture behavior of DB specimens is simulated by controlling damage tolerance.

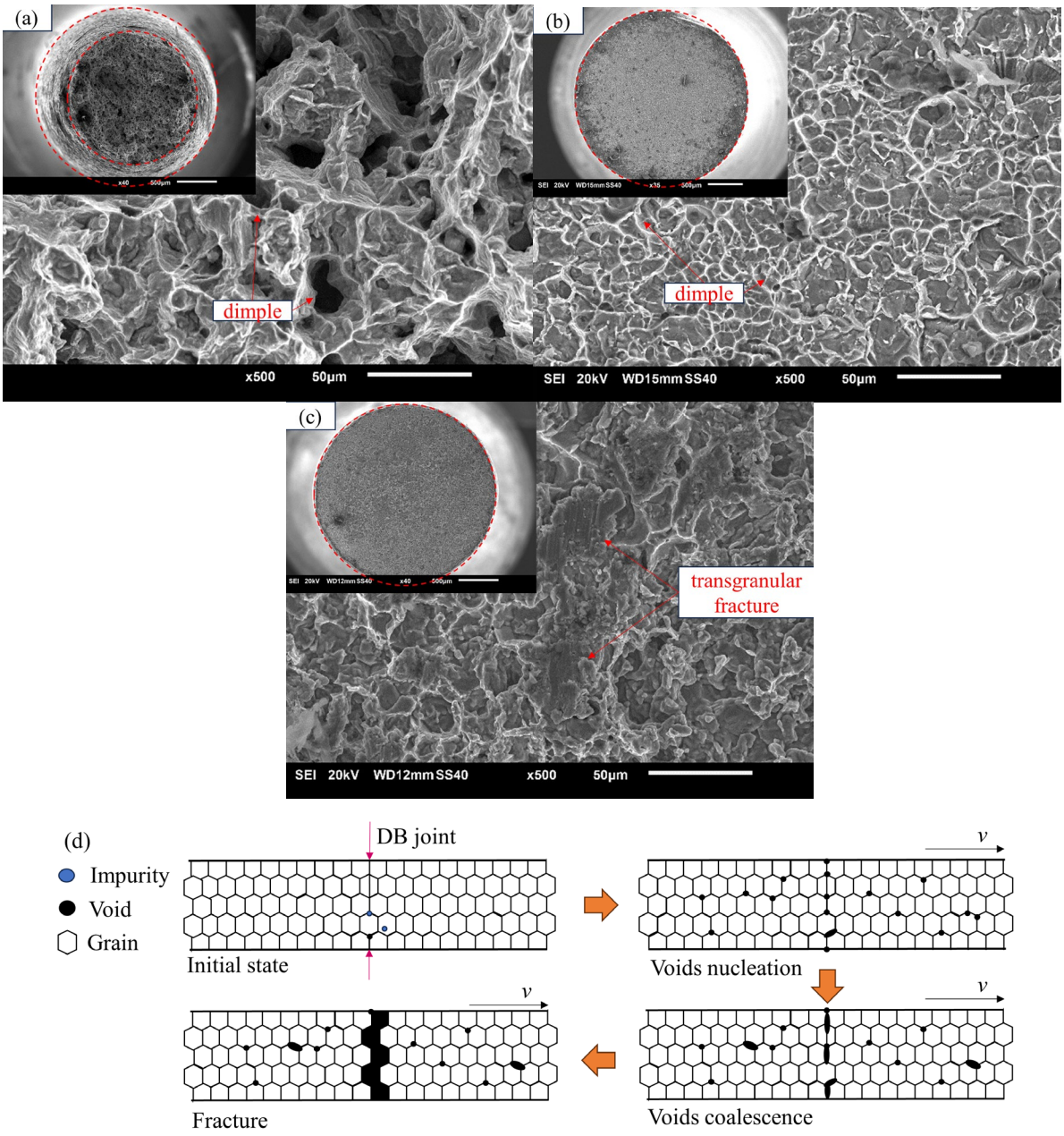

Fig. 3. Fracture (a) BM specimen $0.1s^{-1}$; (b) DB specimen $0.1s^{-1}$; (c) DB specimen $0.001s^{-1}$ and (d) schematic diagram of forming mechanism.

Development of viscoplastic constitutive equations

Viscoplastic flow rule. Lin [10] proposed that the flow stress of a material is mainly composed of three parts: initial yield stress, viscoplastic stress, and hardening stress. The material undergoes

Materials Research Proceedings 44 (2024) 548-557 https://doi.org/10.21741/9781644903254-59

deformation behavior under the synergistic action of the two phases. Therefore, the total plastic strain rate can be expressed as [11]:

$$\begin{cases} \dot{\varepsilon}_{\mathrm{p},\alpha} = \left(\dfrac{\sigma - k_\alpha - H}{K_\alpha} \right)^n \\ \dot{\varepsilon}_{\mathrm{p},\beta} = \left(\dfrac{\sigma - k_\beta - H}{K_\beta} \right)^n \end{cases} . \tag{1}$$

k_α and k_β are the initial yield stress of the α and β phases, respectively. K_α and K_β are the material parameters of the α and β phases, respectively. Based on BAI et al. 's study [11], the relationship between α and β phases can be defined as $k_\alpha = 1.25\, k_\beta$, $K_\alpha = 1.11\, K_\beta$.

The total strain rate is expressed as:

$$\dot{\varepsilon}_p = (1 - f_\beta)\dot{\varepsilon}_{p,\alpha} + f_\beta \dot{\varepsilon}_{p,\beta} . \tag{2}$$

Hardening mechanism. H is the hardening stress due to the evolution of dislocation density during plastic deformation. After extensive experimental verification, its value is known to satisfy the Taylor model. The normalized dislocation density has a value between 0 and 1. Eq. (3) can be obtained by simplifying:

$$H = B\overline{\rho}^{0.5} . \tag{3}$$

B is the isotropic hardening constant, and $\overline{\rho}$ is the relative dislocation density.

Dislocation evolution and softening mechanisms. The dislocation density is elevated, which in turn drives the onset of DRV and DRX behavior, and the reciprocal cancellation of heterogeneous dislocations leads to a decrease in dislocation density. Therefore, the dislocation density evolution equation is expressed as [12]:

$$\frac{d\rho}{d\varepsilon_p} = k\sqrt{\rho} - k_1 \rho . \tag{4}$$

where ε_p is the plastic strain, and k and k_1 are material constants. The first term is related to the dislocation multiplication as a result of plastic straining. The second term models the reduction of dislocation density due to DRV. Since the effects of static recovery and recrystallization on the dislocation density during deformation should not be neglected. The dislocation accumulation and ablation are different for different strain rates at hot temperatures [13]. The strain rate influence term is introduced and expressed in simplified form:

$$\dot{\overline{\rho}} = A\, \dot{\varepsilon}_p^{\delta_1} \left| \dot{\varepsilon}_p \right| - m_1 \overline{\rho} \dot{\varepsilon}_p^{\delta_2} \left| \dot{\varepsilon}_p \right| - m_2 \overline{\rho}^{\delta_3} - \left[m_3 \overline{\rho} / (1 - S) \right] \dot{S} . \tag{5}$$

The results of Alabort et al [8] define the critical value of dislocation density for DRX behavior occurs. In addition, Lin [14] suggested that there is a reserve period for DRX. There is a relationship between the reserve period and the dislocation density. In summary, the evolution of the DRX fraction is described as:

$$\begin{cases} \dot{S} = q_1[x\overline{\rho} - \overline{\rho}_c(1-S)](1-S)^{q_2}. \\ \dot{x} = q_3(1-x)\overline{\rho}. \\ \overline{\rho}_c = q_4\dot{\varepsilon}_p^{q_5}. \end{cases} \tag{6}$$

where q_1, q_2, q_3, q_4 and q_5 are the material parameter, x is the DRX reserve fraction, and $\overline{\rho}_c$ is the critical dislocation density.

The DRX softening effect be introduced based on Zhao's findings [15], modifying Eq. (2) to read:

$$\dot{\varepsilon}_p = ((1-f_\beta)\dot{\varepsilon}_{p,\alpha} + f_\beta\dot{\varepsilon}_{p,\beta})*1/(1-S). \tag{7}$$

Damage evolution. Some scholars believe that the plastic damage mechanism of α, β duplex titanium alloy is the duplex deformation incoordination [16]. The damage evolution equation is expressed as

$$\dot{D} = d_1(1-D)\,|\,\dot{\varepsilon}_{p,\beta} - \dot{\varepsilon}_{p,\alpha}\,|^{d_2} + \frac{d_6\cosh(d_3\varepsilon_p)}{(1-D)^{d_4}}\dot{\varepsilon}_p^{d_5}. \tag{8}$$

where d_1, d_2, d_3, d_4, d_5 and d_6 are material constant.

The damage is introduced into Eq. (1) and corrected to:

$$\begin{cases} \dot{\varepsilon}_{\mathrm{p},\alpha} = \left(\dfrac{\sigma/(1-D) - k_\alpha - H}{K_\alpha}\right)^n. \\ \dot{\varepsilon}_{\mathrm{p},\beta} = \left(\dfrac{\sigma/(1-D) - k_\beta - H}{K_\beta}\right)^n. \end{cases} \tag{9}$$

Based on the concept of damage tolerance mentioned above, a function is set. When the damage reaches the tolerance level, the material undergoes quasi-cleavage fracture. And set the weld-dependent fracture coefficients to control the fracture behavior. Ultimately, the equation is expressed as:

$$F = \mathrm{sign}(f + \mathrm{abs}(\ln(\mathrm{fix}(1000*\mathrm{D})/\mathrm{fix}(\omega)))). \tag{10}$$

where F is the weld-dependent fracture coefficient and ω is the damage tolerance coefficient. f is the material state coefficient: when f is 1, the material state is determined to be BM; when f is 0, the material state is determined to be DB.

The coupled the weld-dependent fracture coefficients, the stresses can be expressed as:

$$\sigma = (1-D)E\left(\varepsilon_T - \varepsilon_p\right)*F. \tag{11}$$

Determination of model parameters. There are many parameters, which are difficult to realize by conventional solution methods. In this paper, the PSO algorithm is used to optimize the parameters. According to the research results of LIN [17] is used as the optimization objective. First, assuming an initial value of dislocation density is 0.1, The experimental data of BM are fitted to the determining parameter. The initial dislocation density is then set to 0 and the damage tolerance coefficient is controlled to obtain accurate DB fracture behavior. The damage tolerance coefficients at different strain rates are plotted as shown in Fig. 4. A linear relationship is met. The

coefficient is obtained by linear fitting. The final expression for the damage tolerance coefficient is obtained as Eq.12. Finally, the parameters are shown in Table 1.

$$\omega = w1 + w2 * \dot{\varepsilon}_T \,. \tag{12}$$

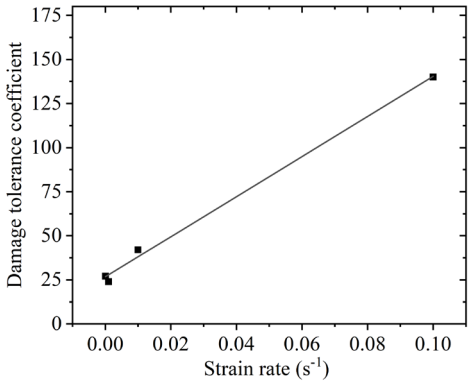

Fig. 4. Damage tolerance coefficient ω value fitting.

Table 1. Optimized values of equation parameters.

E	6.5671e+4	m_2	7.0570	d_4	1.0000	δ_1	0.2495
k_α	1.3736e-7	m_3	1.7013	d_5	1.7322	δ_2	8.1352
K_α	397. 0950	d_1	0.0024	d_6	1.0000	δ_3	6.3147
n	6.9572	d_2	5.5277	A	2.2699	f_β	0.1214
m_1	0.0521	d_3	10.0000	B	93.4351	q_1	0.0363
q_2	1.2703	q_3	6.1014	q_4	4.0477	q_5	3.0832
w_1	26.6744	w_2	1136.8338				

Model application and discussions

Fig. 5(a) shows the comparison between the BM prediction curve (line) and the experimental value (symbol) of BM. The predicted stress values are in good agreement with the experimental values. To quantitatively describe the predictive effect of the model, it was evaluated by statistical methods. The correlation coefficient (R), the average absolute relative error (AARE), and the root mean square error (RMSE) are 0.9933, 3.4%, and 8.1 MPa, respectively. Fig. 5(c) shows the comparison of fracture strain experiment and prediction, and the maximum error is -5.23%. It shows that the model has high accuracy in predicting fracture behavior under MC parameters.

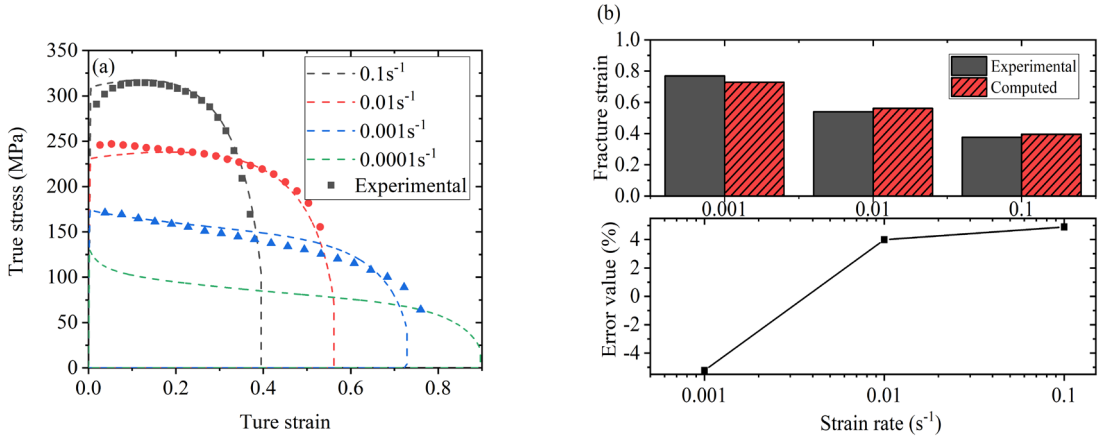

Fig. 5. (a) Stress prediction of BM specimen and (b) fracture strain prediction.

Fig. 6(a) shows the comparison between the BM prediction curve (line) and the experimental value (symbol) of DB. R, AARE, and RMSE are 0.9951,38.1%, and 12.3MPa, respectively. It is shown that the model is also highly accurate in predicting the stresses for the DB state. Fig. 6(c) shows the comparison of fracture strain experiment and prediction, and the maximum error is -3.34%.

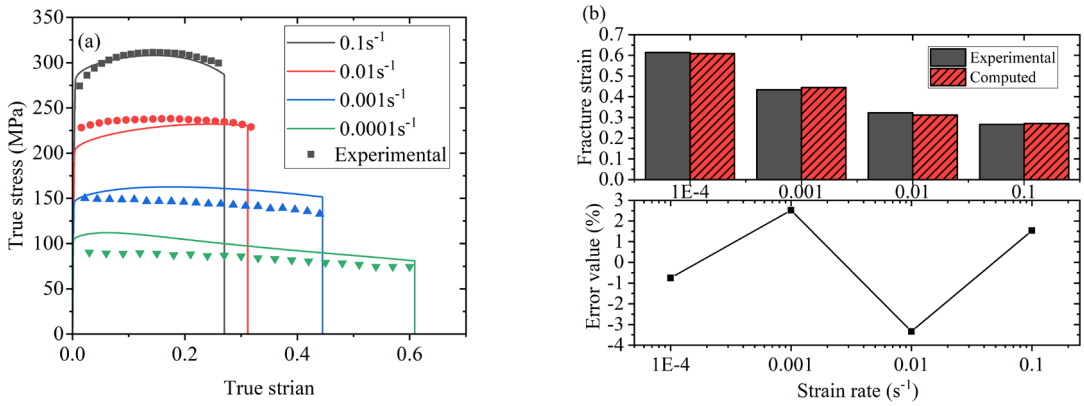

Fig. 6. (a) Stress prediction of DB specimen and (b) fracture strain prediction.

Fig. 7 shows the evolution of the internal variables for BM and DB at $0.001s^{-1}$. It is worth noting that differences in the initial dislocations make a difference in the evolution of the dislocation. It is shown that the higher initial dislocation density of the BM leads to earlier completion of the reserve fraction. This also contributes to earlier and fuller DRX. BM has a higher DRX fraction relative to DB, which is also consistent with the results of the previous stress-strain curves analysis.

At the beginning of deformation, the damage increases relatively slowly and voids nucleate. When the deformation reaches a certain level, a large number of voids begin to coalesce. This causes the damage to grow dramatically until the material breaks. For DB material, the voids are more inclined to the nucleate and coalescence at the DB interface. Most of the damage is concentrated at the DB interface, leading to fracture behavior at small damage values. This is consistent with the experimental performance obtained. According to the above analysis, the prediction of internal variable evolution in the model is also effective.

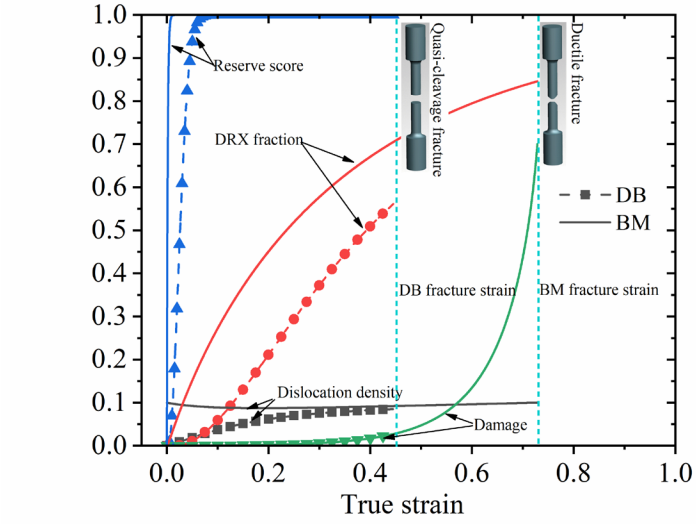

Fig. 7. Evolution of internal variables at $0.001s^{-1}$.

Summary

The thermal deformation behavior of TC4 with and without DB is studied by tensile experiments. The influence of DB structure on thermal deformation behavior is analyzed. A set of internal variable constitutive model considering DB structure is developed and its prediction accuracy is verified. The main conclusions are:

At 750℃, 0.1 ~ 0.0001 s^{-1}, TC4 with DB shows smaller peak stresses during tensile tests than the one without DB, while the fracture strain is smaller, which would greatly affect the forming properties of the DB material.

At 750℃, 0.1-0.0001s^{-1}, the fracture type of TC4 without DB is a ductile fracture and the fracture type of TC4 with DB is a quasi-cleavage fracture. Only a dimple was found in TC4 without DB fracture, while TC4 with DB fracture consists of two structures: transgranular fracture and dimple. The formation mechanism of TC4 quasi-cleavage fracture was expounded as a straight grain boundary formed by incomplete recrystallization and insufficient grain boundary migration energy and the joints weak left over from the DB process caused rapid voids nucleation at the DB interface. The shorter distance of voids coalescence within the interface leads to quasi-cleavage fracture.

By introducing the weld-dependent fracture coefficients and damage tolerance coefficient setting, a unified constitutive model was constructed to describe the hot deformation characteristics of both TC4 with and without DB. The model is capable of describing the evolution of dislocation density, reserve fraction, DRX fractions and damage variables. It can accurately predict TC4 with and without DB stress-strain curves. Within the predicted fracture strain, the prediction accuracy of TC4 without DB statistics: R is 0.9933. The prediction accuracy of TC4 with DB statistics: R is 0.9955. The fracture strain accuracy of TC4 with and without DB is within 3.5,5.5% respectively. It shows that the constitutive model can accurately predict the hot deformation characteristics of TC4 with and without DB at the same time.

References

[1] K. Zheng, D. Li, H. Chen, S. Qu, Z. Zhao, Y. Zhang, Y. Li, Effect of cooling rate on the phase transformation and post strength of Ti-6Al-4V under hot forming conditions: Experiments and modelling, J. Alloy. Compd. 972 (2024) 172868. https://doi.org/10.1016/j.jallcom.2023.172868

[2] Y. Li, H. Chen, L. Du, F. Yang, Y. Zhang, D. Li, Characterization and unified modelling of creep and viscoplasticity deformation of titanium alloy at elevated temperature, Int. J. Plast. (2024) 103892. https://doi.org/10.1016/j.ijplas.2024.103892

[3] C. Li, Y. Li, D. Zhang, X. Li, W. Zhao, Experimental investigation of the mechanical properties and microstructures of Ti–6Al–4V solid-state diffusion bonding joint under high temperature conditions, J. Mater. Res. Technol. 26 (2023) 4042-4058. https://doi.org/10.1016/j.jmrt.2023.08.172

[4] S.V.S. Narayana Murty, B. Nageswara Rao, B.P. Kashyap, Processing maps for hot deformation of α 2 aluminide alloy Ti-24Al-11Nb, J. Mater. Sci. 37 (2002) 1197-1201. https://doi.org/10.1023/A:1014323723598

[5] Y. Peng, J. Li, Z. Li, S. Li, W. Guo, X. Gao, J. Xiong, Interfacial voids and microstructure evolution, bonding behavior and deformation mechanism of TC4 diffusion bonded joints, J. Manuf. Process. 81 (2022) 837-851.

[6] S.M. Imran, C. Li, L. Lang, Y. Guo, H.A. Mirza, F. Haq, S. Alexandrova, J. Jiang, H. Han, An investigation into Arrhenius type constitutive models to predict complex hot deformation behavior of TC4 alloy having bimodal microstructure, Materials Today Commun. 31 (2022)

103622. https://doi.org/10.1016/j.mtcomm.2022.103622

[7] C. Li, I. Sardar Muhammad, L. Lang, Y. Guo, X. Li, S. Alexandrova, D. Zhang, Hot deformation behavior and strain compensation constitutive model of equiaxed fine grain diffusion-welded micro-duplex TC4 titanium alloy, Chinese J. Aeronautics 36 (2023) 510-522. https://doi.org/10.1016/j.cja.2022.07.025

[8] E. Alabort, D. Putman, R.C. Reed, Superplasticity in Ti–6Al–4V: Characterisation, modelling and applications, Acta Mater. 95 (2015) 428-442. https://doi.org/10.1016/j.actamat.2015.04.056

[9] D. Wu, K. Wang, B. Liu, H. Qu, X. Wang, G. Liu, Damage evolution of titanium alloy laser-welded joint during hot deformation: Experiment and modeling, J. Mater. Res. Technol. 26 (2023) 6375-6388. https://doi.org/10.1016/j.jmrt.2023.09.023

[10] B.H. Cheong, J. Lin, A.A. Ball, Modelling of hardening due to grain growth for a superplastic alloy, J. Mater. Process. Technol. 119 (2001) 361-365. https://doi.org/10.1016/S0924-0136(01)00929-3

[11] Q. Bai, J. Lin, T.A. Dean, D.S. Balint, T. Gao, Z. Zhang, Modelling of dominant softening mechanisms for Ti-6Al-4V in steady state hot forming conditions, Mater. Sci. Eng. A 559 (2013) 352-358. https://doi.org/10.1016/j.msea.2012.08.110

[12] Y. Estrin, Dislocation theory based constitutive modelling: foundations and applications, J. Mater. Process. Technol. 80-81 (1998) 33-39. https://doi.org/10.1016/S0924-0136(98)00208-8

[13] Y. Wu, D. Wang, Z. Liu, G. Liu, A unified internal state variable material model for Ti2AlNb-alloy and its applications in hot gas forming, Int. J. Mech. Sci. 164 (2019) 105126. https://doi.org/10.1016/j.ijmecsci.2019.105126

[14] Y. Huo, J. Lin, Q. Bai, B. Wang, X. Tang, H. Ji, Prediction of microstructure and ductile damage of a high-speed railway axle steel during cross wedge rolling, J. Mater. Process. Technol. 239 (2017) 359-369. https://doi.org/10.1016/j.jmatprotec.2016.09.001

[15] L. Zhao, T. Yasmeen, P. Gao, S. Wei, Z. Bai, J. Jiang, J. Lin, Mechanism-based constitutive equations for superplastic forming of TA15 with equiaxed fine grain structure, Procedia Eng. 207 (2017) 1874-1879. https://doi.org/10.1016/j.proeng.2017.10.954

[16] M.A. Greenfield, H. Margolin, The mechanism of void formation, void growth, and tensile fracture in an alloy consisting of two ductile phases, Metall. Mater. Trans. B 3 (1972) 2649-2659. https://doi.org/10.1007/BF02644241

[17] J. Cao, J. Lin, A study on formulation of objective functions for determining material models, Int. J. Mech. Sci. 50 (2008) 193-204. https://doi.org/10.1016/j.ijmecsci.2007.07.003